Propagating Particle Tracking Uncertainty Defined by Fuzzy Numbers in Spatially Variable Velocity Fields

Hauke Blanken, Caterina Valeo, Charles G. Hannah, and Usman T. Khan

2023

Journal of *Marine Science and Engineering*

MDPI

Article

Propagating Particle Tracking Uncertainty Defined by Fuzzy Numbers in Spatially Variable Velocity Fields

Hauke Blanken [1,2,*], Caterina Valeo [2], Charles G. Hannah [1] and Usman T. Khan [3]

[1] Institute of Ocean Sciences, Fisheries and Oceans Canada, Sidney, BC V8L 4B2, Canada; charles.hannah@dfo-mpo.gc.ca
[2] Department of Mechanical Engineering, University of Victoria, Victoria, BC V8P 5C2, Canada; valeo@uvic.ca
[3] Lassonde School of Engineering, York University, Toronto, ON M3J 1P3, Canada; utkhan@yorku.ca
* Correspondence: hauke.blanken@dfo-mpo.gc.ca

Abstract: Accurate prediction of the trajectories of material drifting on the ocean surface is critical for risk assessment and responses to environmental emergencies. Prediction of these trajectories is subject to uncertainty arising from a number of sources, with a primary source being uncertainty in the modelled ocean surface currents and winds used as input to the trajectory model. This article presents a fuzzy number-based algorithm for propagating uncertainty through a particle tracking scheme in a time- and space-varying velocity field. The performance of the algorithm was tested by applying it to idealized, analytical velocity fields and scoring the results against the analytical solution. Both epistemic and aleatoric uncertainty were considered and combined using a fractional Brownian motion model for temporal autocorrelation of the uncertainty. In the evaluation of the algorithm, sensitivity was quantified with respect to parameters such as timestep size, resolution of the forcing velocity field, spatial and temporal gradients in the forcing, and resolution of the applied uncertainty. Parameter values optimizing uncertainty representation and computational cost were identified. The applied uncertainty was found to evolve in agreement with classical relative dispersion relationships.

Keywords: uncertainty; fuzzy numbers; particle tracking

Citation: Blanken, H.; Valeo, C.; Hannah, C.G.; Khan, U.T. Propagating Particle Tracking Uncertainty Defined by Fuzzy Numbers in Spatially Variable Velocity Fields. *J. Mar. Sci. Eng.* **2023**, *11*, 1752. https://doi.org/10.3390/jmse11091752

Academic Editor: Moncho Gomez Gesteira

Received: 5 August 2023
Revised: 31 August 2023
Accepted: 5 September 2023
Published: 7 September 2023

1. Introduction

Accurate prediction of material drift in the ocean is critical for responses to human misadventures in the marine environment, such as oil spill responses and search and rescue operations [1], as well as scientific pursuits, like mapping larval drift and ecosystem connectivity [2]. Drift is forced by the interaction of ocean currents, waves, and winds. These interactions range from simple additive or linearly scaled forcing [3,4] to more complex interactions giving rise to small-scale motions, such as Coriolis–Stokes forcing [5] and submesoscale turbulence [6].

Uncertainty from all sources should be quantified as accurately as possible for accurate drift prediction. Predicted drift trajectories that do not acknowledge the associated uncertainty or include the uncertainty in an improper manner may lead to a range of adverse consequences ranging from improper scientific conclusions to loss of life. It is important to note here that overestimation of uncertainty (i.e., predicting too large a possible search area) may have impacts just as detrimental as underestimation. Steps towards accurate accounting of uncertainty have been taken in, amongst others, previous work by Blanken et al. [7], who employed fuzzy numbers [8–10] to propagate uncertainty through a drift trajectory model forced by time series measured at a single point. However, this work did not consider spatially variable velocity fields and, therefore, the algorithm used by Blanken et al. [7] is not suitable for use with forcing data obtained from numerical models of the ocean and atmosphere. Fuzzy numbers were used in this study since they offer appreciable

benefits in the aggregation of uncertainty from various sources through well-defined arithmetic (cf. [11,12]), can be constructed from a minimum of only three data points, and do not require assumptions about the statistical distribution of the underlying data [13].

Generally, information used to inform drift prediction is obtained from numerical models of currents, wind, and waves, as it is not feasible to measure these parameters at all times with high spatial fidelity. Models, however, are by definition an abstraction of reality and are unlikely to reliably reproduce all physical processes that affect currents, wind, and waves. This is especially true at small spatial and temporal scales, as dynamics at these scales are not well understood and are an active area of research [14]. Misrepresentation of physical processes may be due to assumptions made in the model formulation or due to sub-optimal configuration of the model parameters. Publications such as that by Paquin et al. [15] show that, even in a state-of-the-art ocean modelling system, there is disagreement between modelled currents and those observed in the real world, leading to demonstrated subsequent disagreement between modelled and observed drift trajectories. An example of the implications of this is given in the work by the Canadian Coast Guard [16], who noted that, during the response to a fuel oil spill in the harbour of Vancouver, Canada, three trajectory models were run but none were able to correctly predict the observed trajectory of the spilled oil. The trajectory was reproduced after the fact by Zhong et al. [17], who employed a very-high-resolution hydrodynamic model to provide information on the currents at the time of the incident. Currents were the primary driver of oil drift and dispersion, as there was no significant wind and wave activity in the area at the time. In a general sense, however, results from very-high-resolution hydrodynamic models are unlikely to be readily available in an operational context due to their significant computational expense. Therefore, it is desirable to appropriately account for the uncertainty induced by the use of existing operational ocean models in trajectory prediction.

All instruments used to collect observational data for validating models of the ocean and atmosphere are also subject to uncertainty arising from instrument limitations, limitations in the frequencies of motion resolved in the measurement, and uncertainty in the representativity of the measurements arising from sampling at a finite number of locations. This uncertainty was aggregated for a single observation location and propagated through a trajectory model in the work by Blanken et al. [7].

Other commonly used approaches to uncertainty propagation in drift prediction treat uncertainty as a singular stochastic parameter. This stochastic parameter is often applied by simulating a large number of particles subject to a series of random velocity perturbations drawn from a prescribed distribution; i.e., a random walk [18–20]. More involved approaches have been built on this, such as applying uncertainty to velocity or acceleration rather than position [21] and considering possible persistent autocorrelation in the velocity field by modelling uncertainty as fractional Brownian motion [22,23]. The latter approach is a generalization of a random walk, which is recovered when the fractal dimension of the modelled motion is set to two. Here, strong agreement has been found between the relative dispersion of drifting buoy tracks analyzed via fractional Brownian motion [22] and independent observations of the growth of dye patches in the ocean [24]. For a discrete random walk, uncertainty is expected to grow proportionally to t^3 [25], analogous to the growth rate of a particle cloud in a turbulent field as first described by Richardson [26]. Growth rates are expected to be slower when correlation in the velocity field exists, as was noted by Sanderson and Booth [22] and Okubo [24], who both found relative dispersion proportional to $t^{2.34}$.

An empirical alternative is given by the leeway model for object drift [3], which sees widespread use in search and rescue applications. Here, the wind response of a drifting object is described by nine coefficients determined through a regression analysis of the drift motion against wind velocity. Three of these coefficients are error terms used to define a Gaussian distribution that can be sampled for Monte-Carlo simulations to estimate the uncertainty in the prediction [27]. This approach relies on empirical, object-specific coefficients and is therefore limited in its ability to account for new or unknown

object geometries. However, when comparing predictions made for five different types of drifting buoys, it was found to perform similarly to the deterministic, fuzzy-based analysis performed by Blanken et al. [7].

Some efforts have also been made to reduce model uncertainty by applying hyper-ensemble techniques; i.e., combining results from several different ocean and atmospheric models [28–30]. Ensemble approaches may include models that assimilate observed ocean surface velocities, which has been shown to improve representation of modelled surface velocity structure [31]. These approaches show promise, but for operational application, they are limited to areas where multiple model solutions or the capacity for ensemble modelling with parameter perturbation exist.

Irrespective of the chosen method of uncertainty propagation, making an appropriate choice of the parameters describing the applied uncertainty is critical to producing an accurate trajectory simulation. Within the uncertainty characterization, it is desirable to describe the differences between the numerical model fields used to force the trajectory prediction and observations of currents and winds in the region of interest with as much detail as practicable. This is likely to be the primary source of uncertainty, along with the wind response of the drifting object. When using random velocity kicks to apply uncertainty in drift prediction, model–observation differences may be used to inform the magnitude of these kicks, which are generally drawn from an assumed statistical distribution (cf. [3]). However, describing the uncertainty as a fuzzy number offers the benefits that biases in the forcing model are accounted for without additional modification (through the location of the kernel, see Section 2.1) and no distribution needs to be assumed. Using the exact distribution of the data rather than an assumed approximate distribution has been shown to improve results in geophysical modelling applications [32].

In the current paper, work is presented towards treating uncertainty in drift prediction on a per-source basis. Consideration is given to the differences between the modelled current, wind, and wave fields that inform the drift prediction and analogous observations of these parameters. Specifically, an algorithm for propagating such uncertainty in spatially variable flow fields was developed, as was suggested by Blanken et al. [7]. This algorithm was subjected to a sensitivity analysis of free parameters in order to document its performance. The results from the proposed scheme are contextualized within dispersion theory. This is a crucial step in developing a broader framework for using fuzzy numbers to describe and propagate uncertainty through a drift prediction system, as described by Blanken et al. [7]. The current effort builds on work such as that by Ni et al. [33], who used interval analysis to predict drift trajectories. This is similar in spirit to Blanken et al. [7] and the extension of this work in the present paper. However, Ni et al. [33] did not consider spatial or temporal variability in model forcing fields.

2. Materials and Methods

2.1. A Quick Primer on Fuzzy Numbers

Fuzzy numbers are used throughout this paper to describe uncertainty. They were first introduced by Zadeh [9,10] as a method to accurately describe imprecise quantities. A fuzzy number consists of a value that is believed to certainly be a possible value of the quantity being described (the crisp value or kernel), as well as the ranges of the quantity's value considered to be possible at lower degrees of belief. These ranges are described by the membership function as a function of their corresponding degree of belief. Degree of belief is given in the interval $(0, 1]$, with 1 being assigned to the crisp value. The lowest and highest values of the quantity thought to be possible form the support of the fuzzy number. The membership function increases monotonically from the lower bound of the support to the crisp value and then decreases monotonically towards the upper bound of the support.

Fuzzy numbers are weakly related to probability theory through the consistency principle, which states that the degree of belief in a range of possible values of a quantity must be greater than or equal to the probability of this range of values [10]. This does not have a direct impact on the work presented here but is mentioned to contextualize

the work in the broader literature on uncertainty in particle tracking. In the present work, fuzzy numbers are used since their arithmetic is well defined, which allows straightforward and accurate aggregation of uncertainty from various sources and propagation of this uncertainty through complex mathematical models.

To perform arithmetic on fuzzy numbers, they are first discretized into a set of membership levels (also called α-cuts in the literature) [34]. Membership levels are intervals describing the possible values of a fuzzy quantity at a fixed degree of belief. For mathematical models where no terms are repeated, arithmetic can be performed on each membership level separately using interval arithmetic [11]. If terms are repeated in the model to be solved, then interval arithmetic cannot be used as it overestimates the uncertainty in the result due to "double-counting". In these cases, the transformation method can be used to discretize the fuzzy number into array form and the resulting arrays are used to solve the equations using element-wise arithmetic [12]. The work presented in this paper does not directly require fuzzy arithmetic; however, a brief summary is again presented for context. For further discussion in the context of ocean particle tracking, please refer to [7]. For general discussion of fuzzy mathematics, the reader is referred to the foundational papers [8–10], as well as texts such as [11,12].

2.2. Uncertainty and Fractional Brownian Motion

To propagate uncertainties expressed as fuzzy numbers through drift trajectory predictions, the crisp velocity fields used to force a trajectory model will be perturbed in a systematic manner based on the prescribed uncertainty. For the purpose of this paper, when describing the method for uncertainty propagation, these fields are arbitrarily defined. Rigorous definition of the uncertainty fields based on oceanographic principles is not the focus of the present paper but is discussed in the context of fuzzy numbers in Blanken et al. [7] and will be further discussed in future publications.

Broadly, uncertainty is defined as consisting of an epistemic (or global) component, σ, and an aleatoric (or local) component, σ_l. The epistemic component of uncertainty relates to broad systemic uncertainties arising from the model configuration, while the aleatoric component relates to changes in this uncertainty over the course of the simulation due to internal variability, such as turbulence, numerical noise, and fluctuations in instrument noise in observations. Contributions to the epistemic component of uncertainty in a particle tracking model come from the following sources: the deviations between the hydrodynamic and atmospheric models providing information on the current, wind, and wave fields (the input models) and analogous observations of these fields; unresolved spatial and temporal scales of motion in the input models and observations; instrument uncertainty in the equipment used to make observations of the input fields; and interpolation error due to the finite size of the model input grids.

In this paper, we describe uncertainty as a fuzzy number [8–10] with five membership levels [34] corresponding to values of $\sigma = 0, 0.025, 0.05, 0.075, 0.1$ (which is equivalent to signal-to-noise ratios of $\infty, 40, 20, 13.\overline{3}, 10$). For each membership level, the corresponding value of σ is mapped into (u, v)-space by taking the following in polar coordinates and converting to Cartesian, resulting in the membership function shown in Figure 1.

$$\begin{aligned} (v_r, v_\theta) &= (\sigma, \theta \in [\theta_1, \theta_2, \ldots, \theta_{N_g}]) \\ u &= u_r cos(u_\theta) \\ v &= u_r sin(u_\theta) \end{aligned} \tag{1}$$

The aleatoric component is related to the rate of change in uncertainty, which is in turn related to the autocorrelation of the deviations between the input model fields and analogous observations. If the autocorrelation of these deviations decays exponentially in time then the aleatoric component of uncertainty is equivalent to Brownian motion with the same magnitude as the epistemic uncertainty. For generality, we model the aleatoric uncertainty as a fractional Brownian function [22,35,36]. While continuous solutions to

fuzzy fractional systems exist and recent advances have been made in the field (cf. [37–39]), we consider a discrete solution and exploit the self-similar properties of these functions. In the literature, this self-similarity is given as follows:

$$x(t + \lambda\Delta t) - x(t) \overset{d}{=} \lambda^{\frac{1}{D}}[x(t + \Delta t) - x(t)] \tag{2}$$

Here, $\overset{d}{=}$ implies equality of statistical properties. Therefore, self-similarity suggests that statistically the changes in a time series $x(t)$ over an arbitrary interval Δt are the same as those over an interval $\lambda\Delta t$ if they are scaled by a factor $\lambda^{\frac{1}{D}}$. For a two-dimensional process D, the fractal dimension of the process lies in the interval $1 < D \leq 2$. A value of $D = 1$ implies motion in a straight line, while $D = 2$ implies random motion that eventually fills the available space completely. For the case of $D = 2$, fractional Brownian motion reduces to standard Brownian motion [22]. As the fractal dimension of the uncertainty in drift velocity for a modelled particle is not known a priori, we tested values in the interval $(1, 2]$.

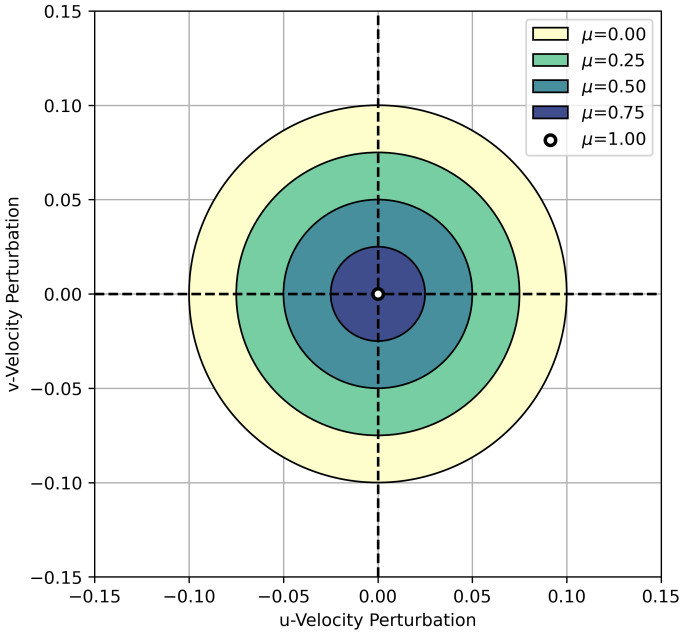

Figure 1. Membership, μ, function of velocity perturbations σ.

If we take $x(t)$ to be the positional uncertainty of a particle in a simulation with length T and the timestep of the simulation to be $\Delta t = \lambda T$, then we can write the following power law for the aleatoric uncertainty, σ_l, in terms of the epistemic uncertainty, σ.

$$\sigma_l = \sigma\left(\frac{\Delta t}{T}\right)^{\frac{1}{D}} \tag{3}$$

As such, for $D = 1$, σ_l evolves as a linear function of the timestep fraction ($\frac{\Delta t}{T}$), while for $D = 2$, the evolution is inverse parabolic with large changes in σ_l at small timestep fractions and comparatively smaller changes at large timestep fractions. Details on the application of the uncertainty described in this section to perturb the forcing velocity field are given in Section 2.4.

2.3. Forcing Field

The crisp velocities to be perturbed by the uncertainty described in the previous section are given by two idealized, analytical vector fields (Figure 2). Both represent a variation of a counterclockwise rotating monopole vortex. The first field under consideration is the

simplest one, representing the vortex in steady form with constant angular velocities. In mathematical form,

$$\begin{aligned} V_r(t,r,\theta) &= 0 \\ V_\theta(t,r,\theta) &= sin(\frac{\pi r}{2}) \end{aligned} \tag{4}$$

Here, v_r is the radial velocity and v_θ is the angular velocity. All other symbols are as conventionally defined in polar coordinates.

The second field was designed to test performance in unsteady velocity fields; here, a periodically reversing flow. The magnitude of angular velocity varies sinusoidally with time t.

$$\begin{aligned} V_r(t,r,\theta) &= 0 \\ V_\theta(t,r,\theta) &= cos(t+\frac{1}{2})sin(\frac{\pi r}{2}) \end{aligned} \tag{5}$$

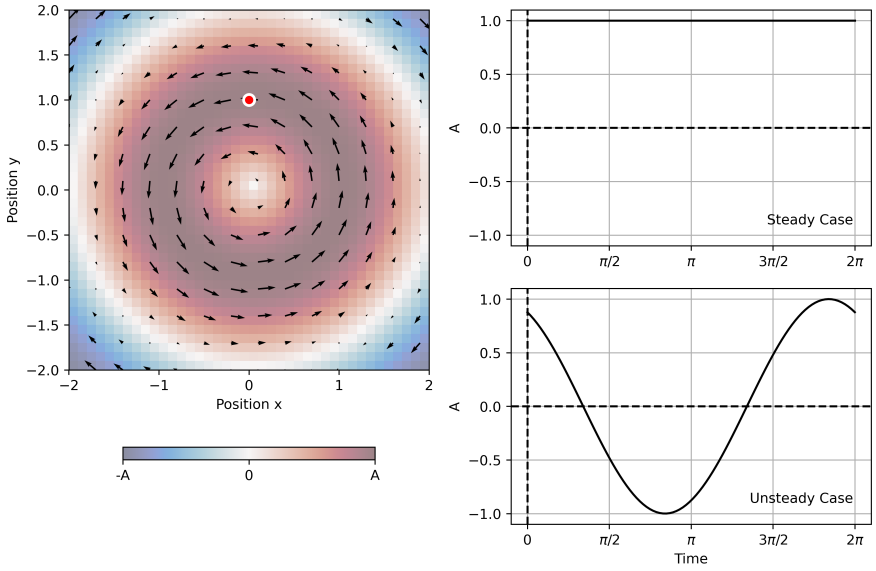

Figure 2. Analytical velocity fields used in this study. Both fields consider a counterclockwise rotating monopole vortex with amplitude A (**left panel**). In the steady case, A is held constant at 1 (**top right panel**). In the unsteady case, A varies sinusoidally with time with an amplitude of 1 (**bottom right panel**).

For the purpose of this paper, particle tracking is started at (x_0, y_0) = (0,1) and completed for a duration of $T = 2\pi$. For the constant velocity case, this duration implies that the analytical solution completes one full rotation around the vortex.

2.4. Fuzzy Particle Tracking

Particle tracking is conducted in two loops: an outer loop over the membership levels of the fuzzy number describing velocity uncertainty (Figures 1 and 3A) and an inner loop over the number of timesteps required to reach the end of the simulation (orange outlined area in Figure 3).

The outer loop begins by determining σ_l based on the value of σ corresponding to the membership level under consideration and the prescribed values of the timestep (Δt), simulation length (T), and fractal dimension of the uncertainty (D) in accordance with Equation (3). The area in u/v—space described by σ and σ_l is then discretized into a set of possible perturbations. The discretization of σ is done on a grid of size $N_g \times N_g$, resulting in M possible perturbations. Similarly, σ_l is discretized on a $N_l \times N_l$ grid, resulting in K possible per-timestep perturbations (panels B1 and B2 of Figure 3). N_g and N_l are free parameters of the simulation. The simulation then proceeds to the inner loop, which is run over $N = \frac{T}{\Delta t}$ timesteps.

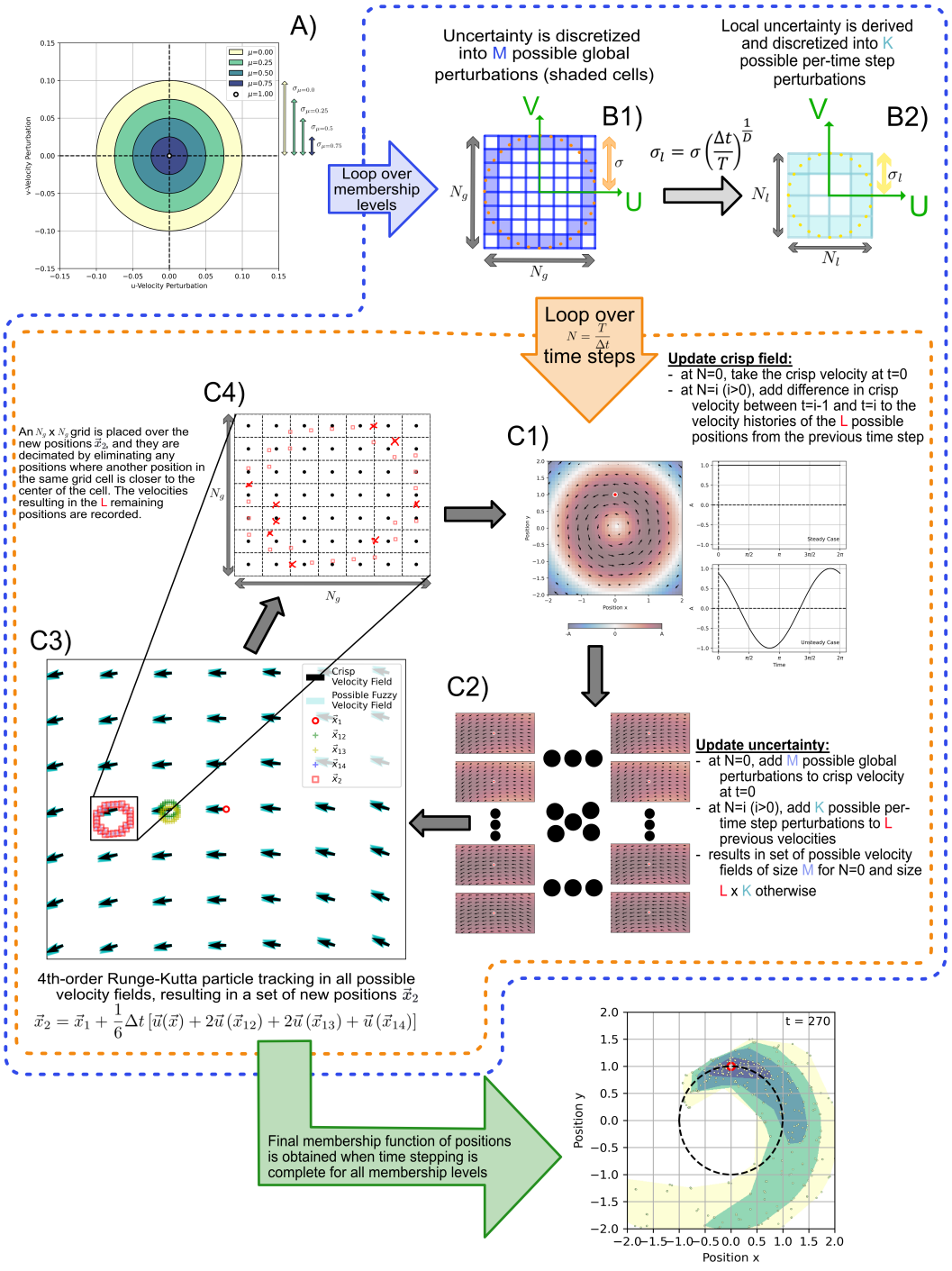

Figure 3. Schematic showing the fuzzy particle tracking scheme described in Section 2.4. Epistemic uncertainty σ is given by the fuzzy number introduced in Section 2.2 (Figure 1, reproduced in panel **A**) and for each membership level is discretized into a set of possible perturbations (panel **B1**). Aleatoric uncertainty is derived from Equation (3), and discretized into possible perturbations as shown in panel **B2**. For each membership level, the set of possible positions is derived by looping over the following steps until the end of the simulation: (1) update the crisp velocity field (panel **C1**); (2) update the uncertainty based on discretized epistemic (first step) and aleatoric (subsequent steps) uncertainty (panel **C2**); (3) advance all possible positions by integrating possible velocity fields (panel **C3**); (4) eliminate extraneous solutions (red x's in panel **C4**). The membership function of possible final positions is obtained when this loop is complete for all membership levels (**bottom panel**).

For the first two steps of the inner loop, we begin by describing the procedure on the first iteration ($N = 0$) as this presents a special case. Here, the epistemic uncertainty, represented by σ, is introduced. Initially, the crisp velocity is updated (panel C1 of Figure 3) to be the value of the crisp velocity field interpolated to (x_0, y_0). Following this, the possible perturbations of this crisp value are individually added to the crisp velocity to produce a set of possible velocity fields (panel C2 of Figure 3). For the first iteration, this means that the M possible perturbations discretized from σ at the beginning of the outer loop are added to the crisp velocity at (x_0, y_0) to produce M possible velocity fields.

Particles are then advanced by one timestep from their position in each of the possible velocity fields using a fourth-order Runge–Kutta integration scheme with inverse distance-weighted interpolation (panel C3 of Figure 3). For the interpolation, the search radius is set to 0.1 and the power parameter to 6, as these values were found to optimize the interpolation results. Once the integration is complete and the new positions $\vec{x}_2$ have been obtained for all possible velocity fields, the set of positions $\vec{x}_2$ is decimated to manage computational expense by preventing exponential growth in the number of possible positions considered. The decimation is done by placing a grid of size $N_g \times N_g$ over the positions $\vec{x}_2$ and only keeping the positions that are closest to the center of the grid cell in cells containing multiple possible positions (panel C4 of Figure 3). The velocity fields resulting in the remaining L positions are recorded and passed back to the start of the inner loop for further time stepping.

For subsequent timesteps, the aleatoric uncertainty represented by σ_l is introduced. Here, the crisp velocity is updated by first computing the difference in the crisp velocity field between the current timestep and the previous timestep and then adding this difference to the set of velocity fields resulting in the L possible positions at the end of the previous timestep (panel C1 of Figure 3). Each updated velocity field is then perturbed by K possible per-timestep perturbations (determined from σ_l at the beginning of the outer loop), resulting in a set of $L \times K$ new possible velocity fields to advance each possible position $\vec{x}_2$ (panel C2 of Figure 3). The processes for integration to obtain new possible positions and decimation of these positions for computational efficiency are unchanged from the first timestep to subsequent timesteps.

Once timestepping is complete for all membership levels, the membership function of possible final positions is obtained from the final sets of possible positions $\vec{x}_2$ at each membership level.

The free parameters of the model are the particle tracking timestep (Δt), the resolution of the forcing velocity field (dx), the grid size for discretization of σ (N_g), the grid size for discretization of σ_l (N_l), and the fractal dimension of the uncertainty D. To gain further insight into appropriate values for these parameters, a sensitivity analysis was conducted over a parameter space with bounds determined by the limits of computational stability and the results of the skill assessment discussed in Section 2.5. The timestep Δt was varied from $\frac{2\pi}{360}$ to $\frac{2\pi}{60}$. The timestep is hereafter reported as the denominator of the given values (i.e., 360 for the smallest timestep), and the analytical solution in the constant velocity case is displaced by one degree per timestep. The spatial resolution of the forcing field dx was varied from 1% to 15% of the vortex radius. Larger values of Δt and dx led to instability in the RK4 particle tracking scheme. The minimum values of N_g and N_l were set to 16 and 5, respectively. Below these values, the reliability of the method deteriorated as the decimation of positions (panel C4 of Figure 3) began to fail due to the decimation of too many positions as a result of the large grid and small number of positions. The maximum values of N_g and N_l were set to 64 and 15, respectively, as the skill assessment (Section 2.5) indicated that these maxima for the parameter space would cover the appropriate values. This is further discussed in Sections 3 and 4. The fractal dimension of the uncertainty D should be informed by analysis of the errors to be accounted for; for example, through yardstick analysis [40] of a time series of model–observation differences. Since we have no prior information on the value of this parameter, the entire possible parameter space $D \in (1, 2]$ should be evaluated.

2.5. Skill Assessment

The algorithm presented in this section was evaluated by performing an analysis of sensitivity to variations in $N_g \in [16, 32, 64]$ and $N_l \in [5, 7, 9, 11, 13, 15]$, as well as the particle tracking timestep Δt and the resolution of the forcing velocity field dx. The objective here was to determine the combination of parameters that maximizes model skill while minimizing computational effort. Additionally, the choice of parameters should not diminish the representation of the uncertainty in the final result.

Simulations were performed with each possible combination of parameters and scored using a cost function, written as follows:

$$C = \frac{1}{2} s \left[\frac{T_C}{T_{C_{max}}} + \left(1 - \frac{F}{F_{max}} \right) \right] \tag{6}$$

Here, F is the integral of the membership function of particle position, representing the amount of information on uncertainty contained in the solution. F_{max} is the largest value of F for a specified fractal dimension of aleatoric uncertainty, D. Trajectories are computed for $D \in [1.1, 1.3, 1.5, 1.7, 2]$, and the mean cost from all values of D for a specific parameter combination is reported. T_C is the time required for the simulation to complete on a consumer-grade laptop, with $T_{C_{max}}$ being the value of T_C for the simulation with $F = F_{max}$. Finally, $s = 1 - s_1$, where s_1 is the separation between the crisp numerical solution for the given dt and dx and the analytical solution. Therefore, a value of $s = 1$ indicates that the crisp numerical solution reproduces the analytical solution exactly.

3. Results

3.1. Steady Forcing Field

The proposed particle tracking scheme produced stable results in a steady velocity field for the investigated parameter. The spatial resolution of the velocity field was found not to have a significant impact on the results, and the results that follow were obtained using a spatial resolution of 10% of the vortex radius.

Examining the required computational effort (runtime) and uncertainty content (integral of final position membership function) for simulations in the considered parameter space showed that both uncertainty content and computational expense increased with increased resolution (N_g, N_l) for the uncertainty space (Equation (1)) and decreased timestep (Figure 4). Regarding uncertainty content, the most evident change was with the increase in N_l from 5 to 7 new positions per timestep. Further increases in N_l resulted in comparatively smaller increases in uncertainty content. These patterns were similar but not completely consistent across the investigated values of N_g. A second notable increase in uncertainty content was evident with N_l increasing from 11 to 13 at N_g = 32 and with N_l increasing from 9 to 11 at N_g = 64. Each increase in N_g resulted in an approximate quadrupling of the computational effort required, while increases in N_l increased computational effort by 1.5–3×, with increases being more expensive in the lower range of considered values of N_l. The increase in the range of required computational effort as a function of fractal dimension, D, indicated by the blue shading in Figure 4, was notable with increasing N_g, as broader dispersion at higher values of D resulted in more positions being carried forward (i.e., not decimated) from one timestep to the next when the discretization used in the decimation became increasingly fine (bottom panels of Figure 3 and panel C4 of Figure 3).

In terms of the cost function (Equation (6)) and its individual terms, it became evident that adequate representation of the actual uncertainty in the simulation could only be achieved at higher values of N_g and N_l, with exact values depending on the users' tolerance for unrepresented uncertainty (Figure 5). Cost generally decreased with decreasing timestep, indicating that the additional uncertainty represented at lower timesteps outweighed the increase in computational cost. For most cases, cost varied between ∼0.2 and 0.4. The most complete representation of uncertainty was achieved with the most computationally intensive combination of parameters (largest N_g and N_l and lowest timestep, bottom left panel of Figure 5); however, the strong similarity in uncertainty content for the cases

with $N_g = 64$ and $N_l \in [11, 13, 15]$ is evidence that further increases in N_l would be unlikely to lead to corresponding increases in uncertainty content. Given that the cost function suggests that less computationally intensive parameter values may be more efficient, it is prudent to set a threshold of acceptable unrepresented uncertainty for decreased computational cost. In Figure 5, this threshold is arbitrarily set at 0.2 (dashed line); i.e., a 20% under-representation of uncertainty is considered to be acceptable in order to optimize computational effort. This threshold is met with minimum cost for values of $\Delta t = \frac{2\pi}{360}$, $N_g = 32$, and $N_l = 11$ and, therefore, this can be considered to be the optimal choice of parameters for the present case. Note that the crisp skill is consistent near 0.98 and therefore has minimal impact on the simulation cost.

The evolution of the membership function of particle position (shown for the case of $D = 1.5$ in Figure 6) indicates that uncertainty evolves in a manner such that no membership level covers an excessive portion of the domain. This quality is maintained for all values of D, though the extent of the membership function does increase with D, approaching a random walk for $D = 2$ (not shown). The membership function maintains convexity to within the limit of resolution provided by N_g and N_l. Notable features of the membership function are: the lack of possible positions in the vortex kernel, most likely due to any overshoot in the particle tracking biasing positions towards the slower regions on the outside of the vortex; the elongated nature of membership levels in the direction of motion, again likely due to the rapid drop in crisp velocities away from the vortex peak amplifying the effects of uncertainty added to the peak crisp velocity; and the reversal of particle motion in the lowest two membership levels near the bottom of the domain, as perturbed particles are displaced into the reversing portion of the crisp velocity. These features suggest that the scheme behaves in a physically sound manner.

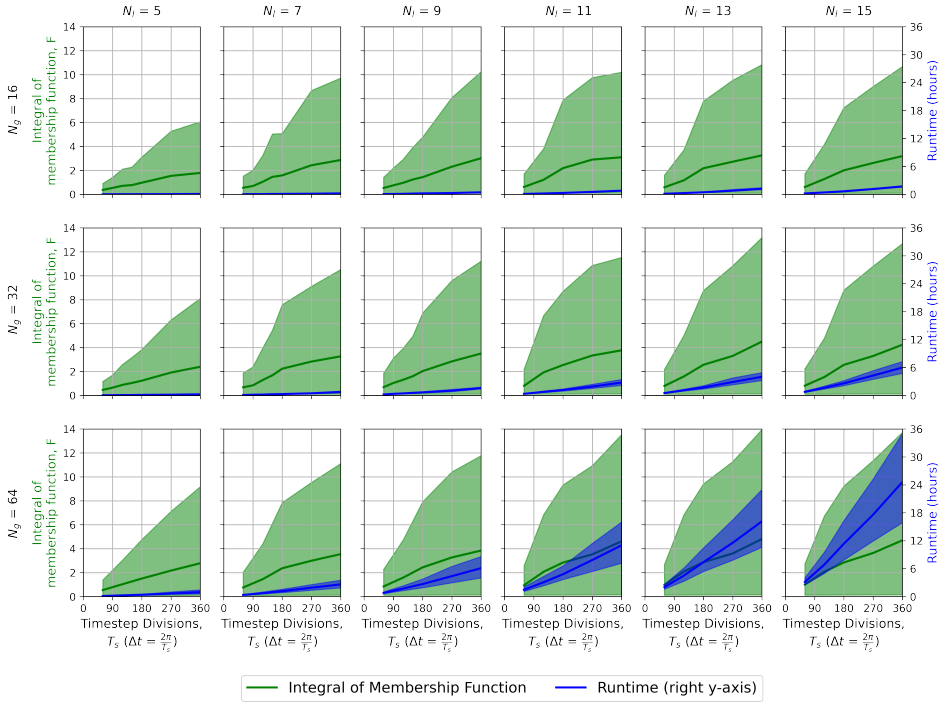

Figure 4. Mean represented uncertainty (green line) given by the integral of the membership function of final positions and computational runtime required (right y-axis, blue line) for simulations in the steady velocity field. Shading indicates the range of values for the examined fractal dimensions, D.

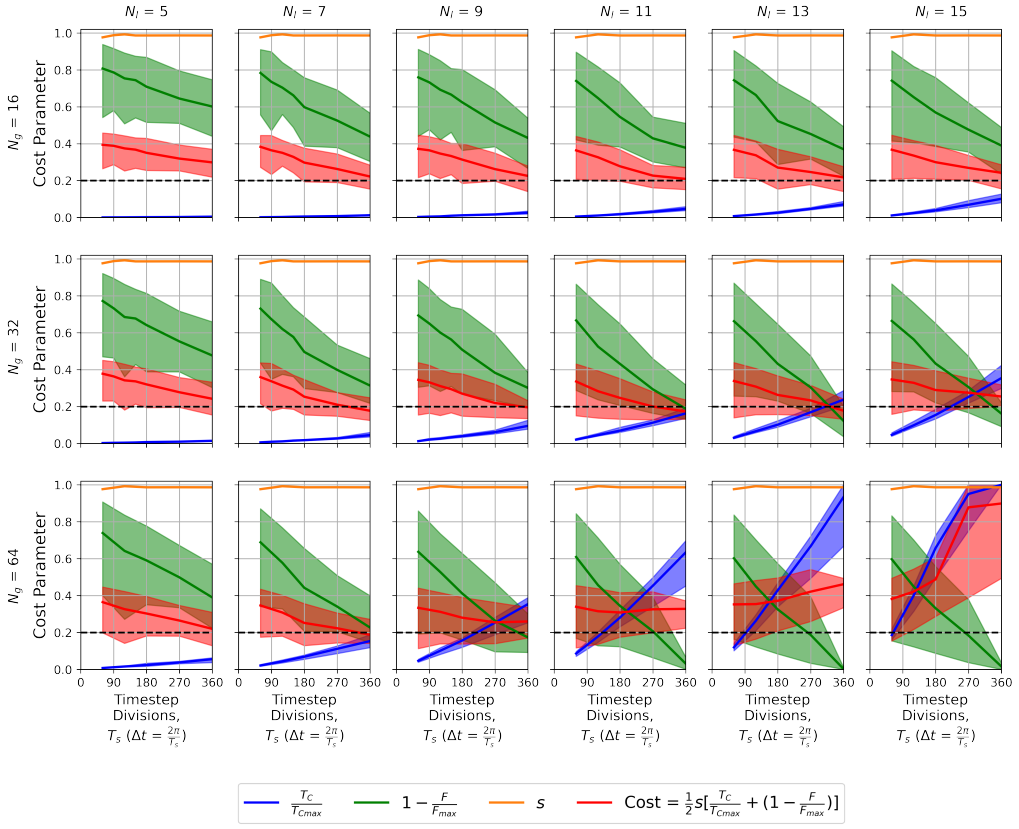

Figure 5. Performance summary for relevant combinations of free model parameters. Plots show mean cost (or components of cost) as a function of timestep for the steady velocity case. Time cost ($T_C/T_{C_{max}}$) is shown in blue, uncertainty cost ($1 - F/F_{max}$) in green, crisp skill (s) in orange, and total cost (Equation (6)) in red. N_g increases from the top to bottom row, and N_l increases from left to right. Shading indicates the range of values for the examined fractal dimensions, D.

3.2. Unsteady Forcing Field

In the unsteady test case, the proposed particle tracking scheme again yielded stable results for the investigated parameter space, with computational characteristics similar to the steady case.

The required computational effort increased slightly compared to the steady case. Increases in N_g increased computational expense by 4.2–4.3×, while increasing N_l increased computational expense by 1.5–3×, as before. The uncertainty content was slightly increased overall, but the relationships observed within the parameter space were generally similar to the steady case (Figure 7).

In terms of the cost function (Equation (6)), cost for the unsteady case was similar or in some cases slightly lower than in the steady case (Figure 8). As for the steady velocity field, the maximum uncertainty content was represented for the cases with $N_g = 64$ and $N_l \in [11, 13, 15]$. Representation of uncertainty content was very similar between these cases, suggesting that further expansion of the parameter space would be unlikely to lead to an increase in uncertainty content. Total cost was again lowest for the case with $N_g = 32$, $N_l = 11$, and timestep division $T_s = 360$. Therefore, this was again considered to be the optimal case.

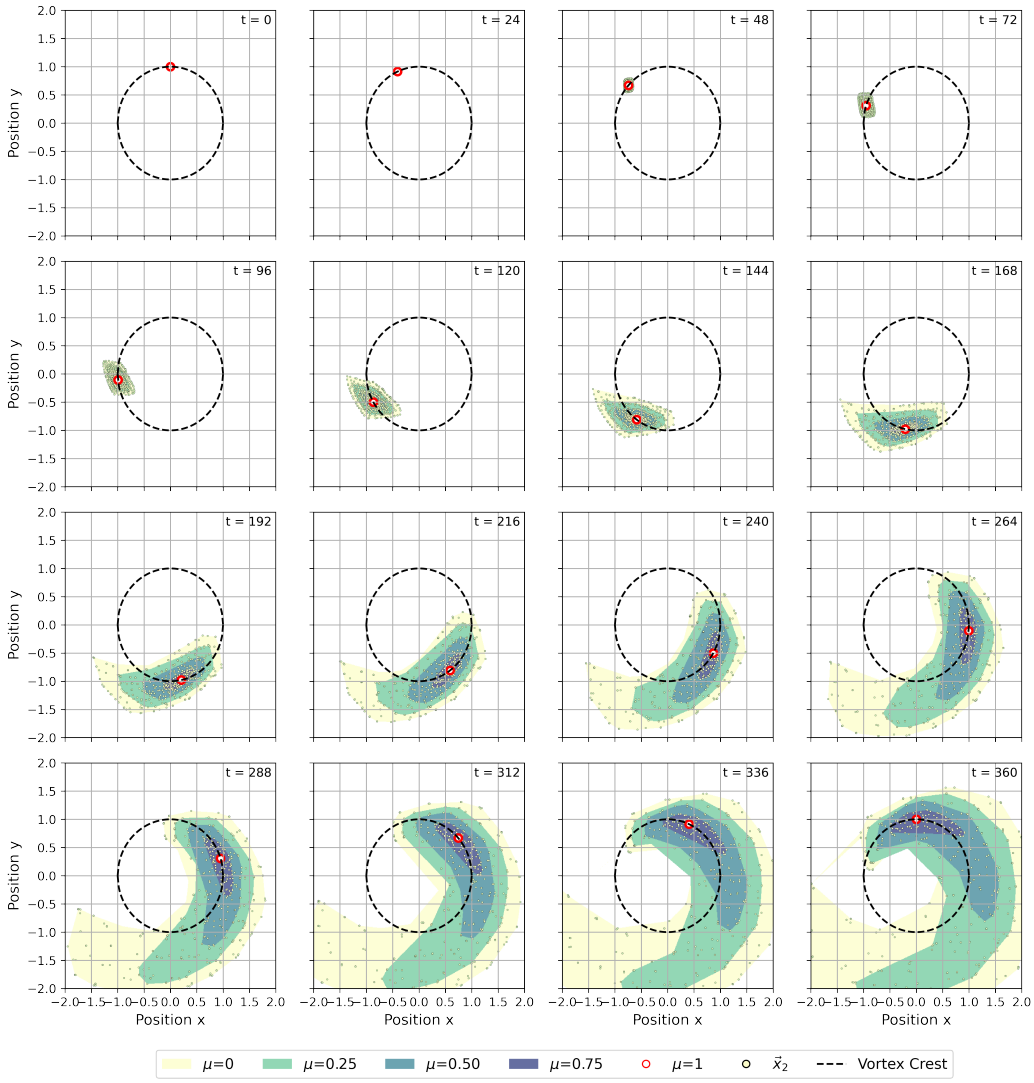

Figure 6. Evolution of particle trajectory for steady velocity case, with $\Delta t = \frac{2\pi}{360}$, $N_g = 32$, $N_l = 11$, and $D = 1.5$. The crisp position is shown by the red and white marker. The membership function of positions is shaded, and individual fuzzy positions are superimposed. The time index of the simulation is given by t (top-right corner of each panel).

For this scenario, the membership function of position (shown for $D = 1.5$ in Figure 9) again indicated stable performance in a qualitatively reasonable manner. Aside from the obvious difference in the crisp velocity field, the isotropy in the membership function was increased, with membership levels showing more significant lateral deviation from the crisp trajectory. This resulted in the membership function encompassing the center of the vortex by the end of the simulation, which was not seen in the steady velocity field. This was likely due to increased directional uncertainty at times when $|A| < 1$. A corollary to this is that the membership function at the final timestep exhibited shallower gradients of possibility (i.e., was more convex) than in the steady velocity field.

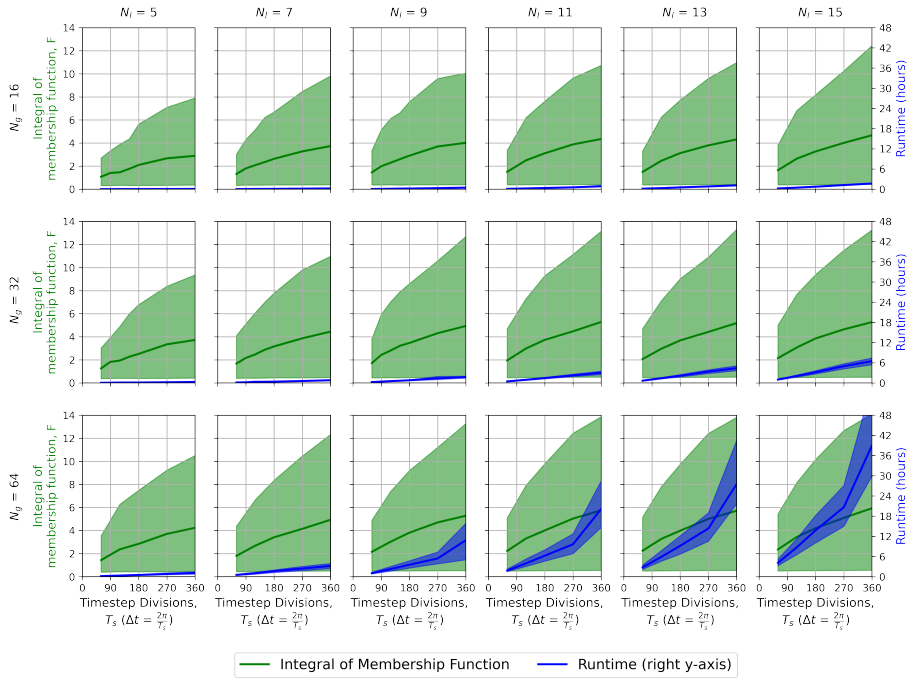

Figure 7. Mean represented uncertainty (green), given by the integral of the membership function of final positions, and computational runtime required (right y-axis, blue) for simulations in the unsteady velocity field. Shading indicates the range of values for the examined fractal dimensions, D.

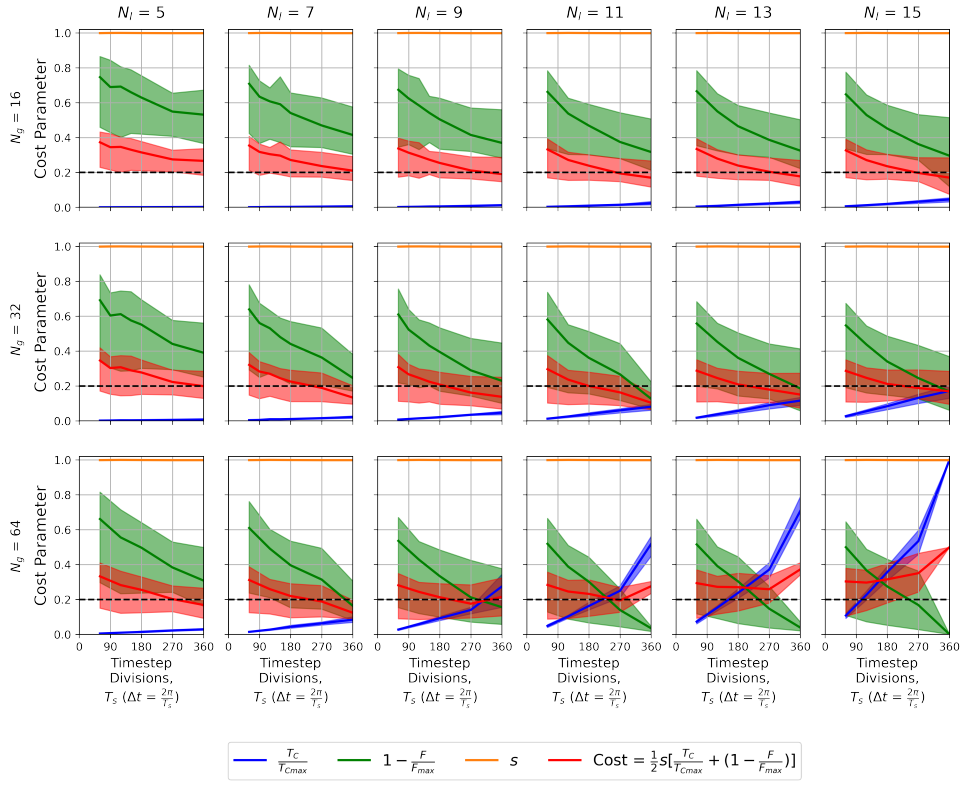

Figure 8. Performance summary for relevant combinations of free model parameters. Plots show mean cost (or components of cost) as a function of timestep for the unsteady velocity case. Time cost ($T_C / T_{C_{max}}$) is shown in blue, uncertainty cost ($1 - F/F_{max}$) in green, crisp skill (s) in orange, and total cost (Equation (6)) in red. N_g increases from the top to bottom row, and N_l increases from left to right. Shading indicates the range of values for the examined fractal dimensions, D.

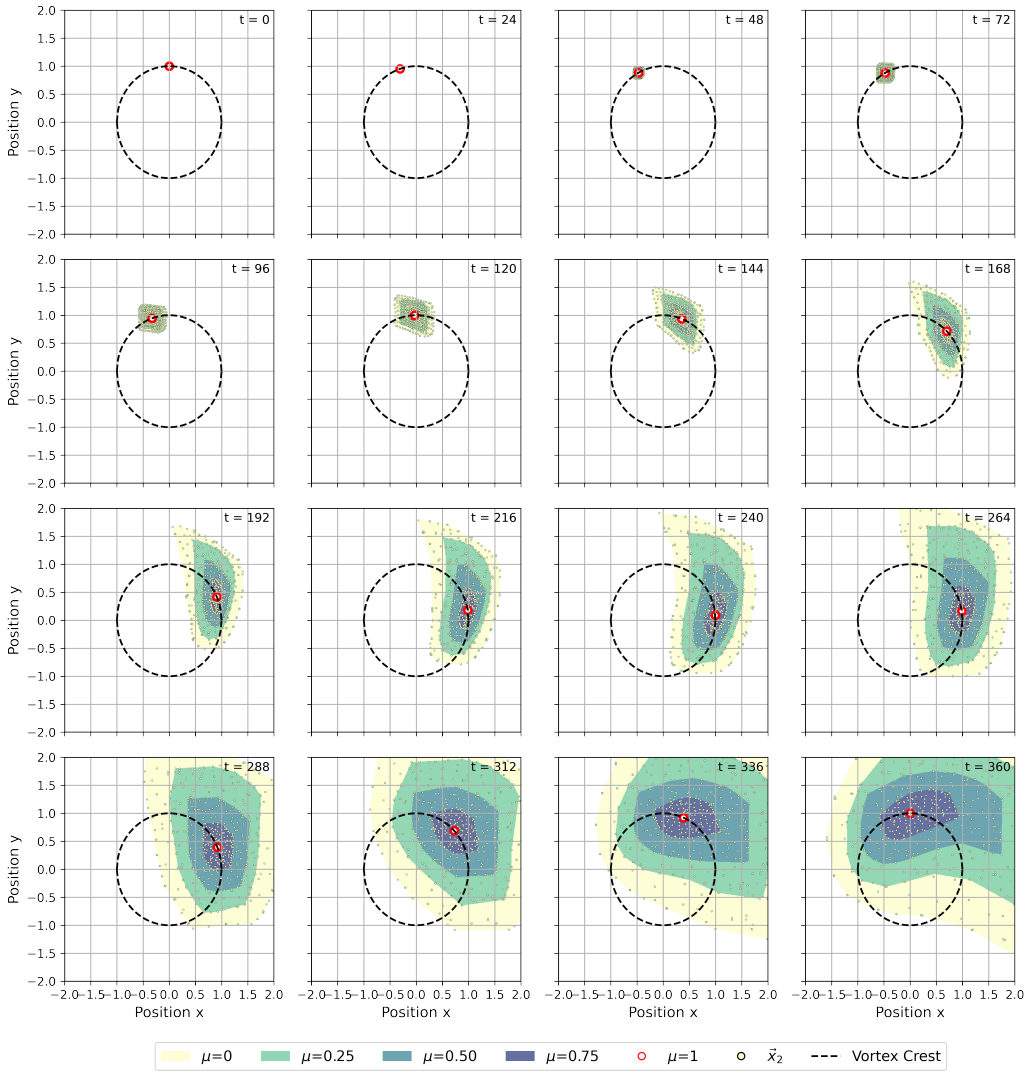

Figure 9. Evolution of particle trajectory for unsteady velocity case, with $\Delta t = \frac{2\pi}{270}$, $N_g = 32$, $N_l = 7$, and $D = 1.5$. The crisp position is shown by the red and white marker. The membership function of positions is shaded, and individual fuzzy positions are superimposed. t (top-right corner of each panel) refers to the time index of the simulation.

4. Discussion

The skill of the method presented here is clearly evident in the very strong correspondence between the crisp numerical solution and the analytical solution (indicated by $s \approx 1$ in Figures 5 and 8), the convergence of represented uncertainty content for increasing values of N_g and N_l, and the physically sound evolution of uncertainty over the course of the simulation. The latter point was evidenced by the characteristics of the trajectory described in the previous section, as well as the fact that the solution remained convex despite membership levels being solved independently of one another (Figures 6 and 9). Further, the amount of uncertainty contained in the simulation increased with D, as was expected from the theory. Therefore, these simulations inspire confidence that the proposed method works in the intended manner.

Therefore, the method above offers the potential to account for uncertainty in the forcing data for a drift trajectory simulation in a systematic and deterministic manner and then propagate this uncertainty through the simulation. The drift trajectory model used by Blanken et al. [7], as well as in many other studies (cf. [4,20,41]), is expressed as follows:

$$\frac{d\vec{x}}{dt} = \vec{u}_c + \vec{u}_s + \alpha\vec{u}_w \tag{7}$$

Here, the drift velocity is $\frac{d\vec{x}}{dt}$, $\vec{u}_c$ is the ocean surface current, $\vec{u}_s$ is the Stokes drift due to the ocean surface wave field, $\vec{u}_w$ is the ocean surface wind, and α is a scaling coefficient. Accounting for uncertainty in this model will require numerical models of the ocean, atmosphere, and surface wave field, as well as observations of surface currents, winds, and waves/Stokes drift to validate the model results. Broadly speaking, for each forcing term, uncertainty can be expressed as a fuzzy number by: (1) mapping the model–observation differences as a histogram in u/v-space and converting this histogram to a fuzzy number using the method described by Khan and Valeo [42]; (2) expressing the uncertainty due to unresolved time scales and instrument uncertainty as fuzzy numbers, as in the work by Blanken et al. [7]; (3) combining the fuzzy numbers from steps one and two using the principles of fuzzy arithmetic [11,12,43]. Uncertainties in the forcing from surface currents, wind, and Stokes drift can then be aggregated using Equation (7) and fuzzy arithmetic to form an overall uncertainty term equivalent to σ in the present study. The crisp forcing field can be similarly derived by combining the modelled forcing fields according to Equation (7). Finally, the individual time series of model–observation differences may be combined according to Equation (7) and the result can be used to determine an appropriate value for D through yardstick or other fractal analysis [36,40,44,45].

Innovations and improvements are expected to arise from this approach through the accurate aggregation of uncertainty from various sources without the need to assume a statistical distribution [32], the accounting for correlations in the error fields through the use of fractional Brownian motion, and the implicit inclusion of any biases in the forcing models. The latter are included through the fuzzification of model–observation differences, which negates any need for biases to be accounted for through dispersion over an artificially large area. It is noted that biases and other uncertainty characteristics are likely to exhibit spatial variability and, therefore, collecting representative observations at as many locations as practicable and repeating the uncertainty quantification at each location is likely to provide significant benefit.

In the present study, analysis of the growth rate of the uncertainty content indicated strong agreement with the theory of relative dispersion; i.e., the growth rate of a dispersing patch of material about its center of mass. For the steady velocity case (Figure 10), uncertainty content was found to grow as $F \propto t^{3.04}$ with $D = 2$, which is consistent with the proportionality to t^3 proposed by [26] and the finding that piecewise-ballistic models of turbulence (functionally similar to the proposed method) exhibit t^3 scaling of relative dispersion [25]. A comprehensive analysis of expected dispersion behaviour for lower values of D and increasing correlation in the velocity increments (higher σ_l) is beyond the scope of the present study. However, it is noted that, for lower values of D, the exponent of time decreases from 3, approaching 2 as D approaches 1. For $D = 1.3$, proportionality of $F \propto t^{2.37}$ was observed, which is consistent with the observation of Sanderson and Booth [22] ($\propto t^{2.34}$) for a similar value of D, as well as those of Okubo [24], who observed this time dependence in dye studies but did not invoke fractal concepts. Therefore, the proposed method appears to be well grounded in physics, reproducing previously observed behaviours of particle separation or patch growth in stochastic fields.

A remaining question is whether the parameter space investigated in Section 3 completely resolves the uncertainty contained in the formulated problem. It is feasible that, even though further improvements in cost are unlikely, further uncertainty may be resolved by considering increased values of N_g and N_l. However, in both the steady and unsteady case, the value of F converges for $N_g = 64$ and $N_l \geq 11$ while computational expense increases drastically. From the local minimum of the cost function at $N_g = 32$, it is evident that further increases in N_g may not be necessary for practical application.

The optimal combination of free parameters in the proposed trajectory model will likely be application-specific. Values given here are for a consumer-grade laptop with a 4.6 GHz processor, 24 Mb cache, and 32 Gb RAM. It is likely that code optimization from the current serial formulation, to make use of parallel processing and/or GPUs, can result in significant improvements in computational speed. Therefore, the metrics for the

computational effort and total given in this paper should be taken as guidelines rather than firm conclusions.

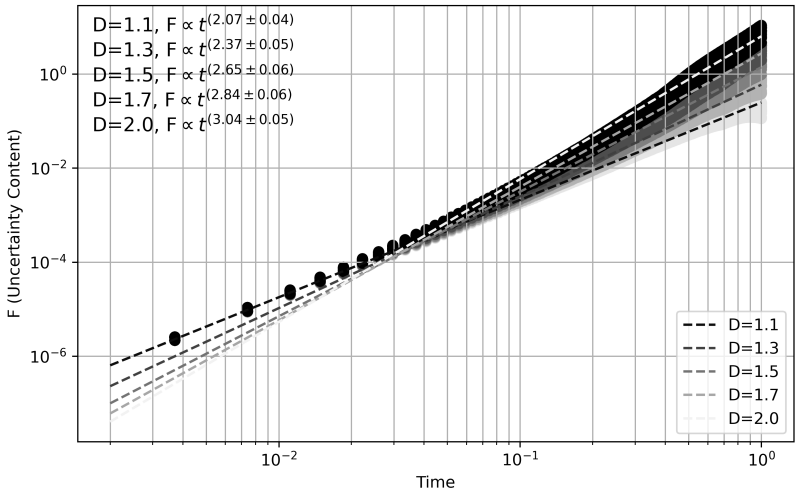

Figure 10. Uncertainty content (F) as a function of time, varying with fractal dimension D. Results are shown for the steady velocity case.

In future studies, this method will be applied to realistic scenarios with accurately described uncertainty to evaluate the performance against real-world observations and traditional models for uncertainty, such as Brownian motion.

5. Conclusions

A method for propagating uncertainty expressed as a fuzzy-valued vector through a particle tracking model in a spatiotemporally variable velocity field was developed and shown to produce realistic results with reasonable computational effort. This addresses a need for fuzzy number-based uncertainty propagation through models for the drift of objects floating on the ocean surface, as described by Blanken et al. [7], as these models are generally forced with spatiotemporally variable output from hydrodynamic, atmospheric, and wave models. Uncertainty description based on fuzzy numbers allows for the consideration of bias and anisotropy with just a small number of input data points and without requiring the assumption of a statistical distribution.

Results regarding the properties of the proposed method can be summarized as follows:

- The crisp solution tracks the analytical solution to within 2% or less in both steady and unsteady velocity fields;
- The modelled uncertainty evolves as expected for the chosen scheme based on fractional Brownian motion. Uncertainty increases with the fractal dimension as more aleatoric uncertainty is admitted into the solution;
- The temporal evolution of the modelled uncertainty corresponds well with classical relative dispersion relationships, both for a fractal dimension of two (Brownian motion) and lower fractal dimensions;
- In terms of the cost function used to evaluate the results of the sensitivity analysis to model free parameters, optimal results in both the steady and unsteady case were achieved for the following parameter combination: $\Delta t = \frac{2\pi}{360}$, $N_g = 32$, $N_l = 11$. Note that this may not be a universal result.

These results inspire confidence that the proposed method will lead to improved uncertainty assessment in ocean surface drift simulations when applied to real-world scenarios with realistic forcing. This will be confirmed in future studies.

Author Contributions: Conceptualization, H.B., C.V. and U.T.K.; methodology, H.B., C.G.H. and C.V.; software, H.B.; validation, H.B. and C.G.H.; formal analysis, H.B., C.V. and C.G.H.; writing—original draft preparation, H.B.; writing—review and editing, C.V., C.G.H. and U.T.K.; visualization, H.B.; supervision, C.V., C.G.H. and U.T.K. All authors have read and agreed to the published version of the manuscript.

Funding: This work was made possible through the oceanography sub-initiative of the Government of Canada's Oceans Protection Plan.

Institutional Review Board Statement: Not applicable.

Informed Consent Statement: Not applicable.

Data Availability Statement: The code for the proposed particle tracking model, along with other scripts generated during the preparation of this manuscript, can be accessed at: https://gitlab.com/haukecblanken/fuzzydrift (accessed on 6 September 2023).

Conflicts of Interest: The authors declare no conflict of interest.

References

1. Davidson, F.J.M.; Allen, A.; Brassington, G.B.; Breivik, Ø.; Daniel, P.; Kamachi, M.; King, B.; Lefevre, F.; Sutton, M.; Kaneko, H. Applications of GODAE Ocean Current Forecasts to Search and Rescue and Ship Routing. *Oceanography* **2009**, *22*, 176–181. [CrossRef]
2. Röhrs, J.; Christensen, K.H.; Vikebø, F.; Sundby, S.; Saetra, Ø.; Broström, G. Wave-induced transport and vertical mixing of pelagic eggs and larvae. *Limnol. Oceanogr.* **2014**, *59*, 1213–1227. [CrossRef]
3. Breivik, Ø.; Allen, A.A. An operational search and rescue model for the Norwegian Sea and the North Sea. *J. Mar. Syst.* **2008**, *69*, 99–113. [CrossRef]
4. Röhrs, J.; Christensen, K.H.; Hole, L.R.; Broström, G.; Drivdal, M.; Sundby, S. Observation-based evaluation of surface wave effects on currents and trajectory forecasts. *Ocean. Dyn.* **2012**, *62*, 1519–1533. [CrossRef]
5. van den Bremer, T.S.; Breivik, Ø. Stokes drift. *Philos. Trans. R. Soc. Math. Phys. Eng. Sci.* **2018**, *376*, 20170104. [CrossRef]
6. Poje, A.C.; Özgökmen, T.M.; Lipphardt, B.L., Jr.; Haus, B.K.; Ryan, E.H.; Haza, A.C.; Jacobs, G.A.; Reniers, A.J.H.M.; Olascoaga, M.J.; Novelli, G.; et al. Submesoscale dispersion in the vicinity of the Deepwater Horizon spill. *Proc. Natl. Acad. Sci. USA* **2014**, *111*, 12693–12698. [CrossRef]
7. Blanken, H.; Valeo, C.; Hannah, C.; Khan, U.T.; Juhász, T. A Fuzzy-Based Framework for Assessing Uncertainty in Drift Prediction Using Observed Currents and Winds. *Front. Mar. Sci.* **2021**, *8*, 618094. [CrossRef]
8. Zadeh, L.A. Fuzzy sets. *Inf. Control.* **1965**, *8*, 338–353. [CrossRef]
9. Zadeh, L.A. The concept of a linguistic variable and its application to approximate reasoning—I. *Inf. Sci.* **1975**, *8*, 199–249. [CrossRef]
10. Zadeh, L.A. Fuzzy sets as a basis for a theory of possibility. *Fuzzy Sets Syst.* **1978**, *1*, 3–28. [CrossRef]
11. Kaufman, A.; Gupta, M.M. *Introduction to Fuzzy Arithmetic, Theory and Application*; Van Nostrand Reinhold: New York, NY, USA, 1985.
12. Hanss, M. *Applied Fuzzy Arithmetic: An Introduction with Engineering Applications*; Springer: Berlin/Heidelberg, Germany, 2005.
13. Khan, U.T.; Valeo, C. Comparing a Bayesian and fuzzy number approach to uncertainty quantification in short-term dissolved oxygen prediction. *J. Environ. Inform.* **2017**, *30*, 1. [CrossRef]
14. D'Asaro, E.A.; Shcherbina, A.Y.; Klymak, J.M.; Molemaker, J.; Novelli, G.; Guigand, C.M.; Haza, A.C.; Haus, B.K.; Ryan, E.H.; Jacobs, G.A.; et al. Ocean convergence and the dispersion of flotsam. *Proc. Natl. Acad. Sci. USA* **2018**, *115*, 1162–1167. [CrossRef] [PubMed]
15. Paquin, J.P.; Lu, Y.; Taylor, S.; Blanken, H.; Marcotte, G.; Hu, X.; Zhai, L.; Higginson, S.; Nudds, S.; Chanut, J. High-resolution modelling of a coastal harbour in the presence of strong tides and significant river runoff. *Ocean. Dyn.* **2020**, *70*, 365–385. [CrossRef]
16. Canadian Coast Guard. *Independent Review of the M/V Marathassa Fuel Oil Spill Environmental Response Operation*; Canadian Coast Guard: Ottawa, ON, Canada, 2015.
17. Zhong, X.; Niu, H.; Wu, Y.; Hannah, C.; Li, S.; King, T. A Modeling Study on the Oil Spill of M/V Marathassa in Vancouver Harbour. *J. Mar. Sci. Eng.* **2018**, *6*, 106. [CrossRef]
18. Zelenke, B.; O'Connor, C.; Barker, C.; Beegle-Krause, C.J.; Eclipse, L. *General NOAA Operational Modelling Environment (GNOME) Technical Documentation*. 2012. Available online: https://repository.library.noaa.gov/view/noaa/2620 (accessed on 30 August 2023).
19. De Dominicis, M.; Pinardi, N.; Zodiatis, G.; Archetti, R. MEDSLIK-II, a Lagrangian marine surface oil spill model for short-term forecasting–Part 2: Numerical simulations and validations. *Geosci. Model Dev.* **2013**, *6*, 1871–1888. [CrossRef]
20. Dagestad, K.F.; Röhrs, J.; Breivik, Ø.; Ådlandsvik, B. OpenDrift v1.0: A generic framework for trajectory modelling. *Geosci. Model Dev.* **2018**, *11*, 1405–1420. [CrossRef]
21. LaCasce, J.H. Statistics from Lagrangian observations. *Prog. Oceanogr.* **2008**, *77*, 1–29. [CrossRef]

22. Sanderson, B.G.; Booth, D.A. The fractal dimension of drifter trajectories and estimates of horizontal eddy-diffusivity. *Tellus* **1991**, *43A*, 334–349. [CrossRef]
23. Guo, W.J.; Wang, Y.X.; Xie, M.X.; Cui, Y.J. Modeling oil spill trajectory in coastal waters based on fractional Brownian motion. *Mar. Pollut. Bull.* **2009**, *58*, 1339–1346. [CrossRef]
24. Okubo, A. Oceanic diffusion diagrams. *Deep. Sea Res.* **1971**, *18*, 789–802. [CrossRef]
25. Thalabard, S.; Krstulovic, G.; Bec, J. Turbulent pair dispersion as a continuous-time random walk. *J. Fluid Mech.* **2014**, *755*, R4. [CrossRef]
26. Richardson, L.F. Atmospheric Diffusion Shown on a Distance-Neighbour Graph. *Proc. R. Soc. London. Ser. Contain. Pap. Math. Phys. Character* **1926**, *110*, 709–737.
27. Breivik, Ø.; Allen, A.A.; Maisondieu, C.; Roth, J.C. Wind-induced drift of objects at sea: The leeway field method. *Appl. Ocean. Res.* **2011**, *33*, 100–109. [CrossRef]
28. Rixen, M.; Ferreira-Coelho, E. Operational surface drift prediction using linear and non-linear hyper-ensemble statistics on atmospheric and ocean models. *J. Mar. Syst.* **2007**, *65*, 105–121. [CrossRef]
29. Rixen, M.; Ferreira-Coelho, E.; Signell, R. Surface drift prediction in the Adriatic Sea using hyper-ensemble statistics on atmospheric, ocean and wave models: Uncertainties and probability distribution areas. *J. Mar. Syst.* **2008**, *69*, 86–98. [CrossRef]
30. Vandenbulcke, L.; Beckers, J.M.; Lenartz, F.; Barth, A.; Poulain, P.M.; Aidonidis, M.; Meyrat, J.; Ardhuin, F.; Tonani, M.; Fratianni, C.; et al. Super-ensemble techniques: Application to surface drift prediction. *Prog. Oceanogr.* **2009**, *82*, 149–167. [CrossRef]
31. Carrier, M.J.; Ngodock, H.; Smith, S.; Jacobs, G.; Muscarella, P.; Ozgokmen, T.; Haus, B.; Lipphardt, B. Impact of Assimilating Ocean Velocity Observations Inferred from Lagrangian Drifter Data Using the NCOM-4DVAR. *Mon. Weather. Rev.* **2014**, *142*, 1509–1524. [CrossRef]
32. He, J.; Valeo, C. Comparative Study of ANNs versus Parametric Methods in Rainfall Frequency Analysis. *J. Hydrol. Eng.* **2009**, *14*, 172–184. [CrossRef]
33. Ni, Z.; Qiu, Z.; Su, T.C. On predicting boat drift for search and rescue. *Ocean. Eng.* **2010**, *37*, 1169–1179. [CrossRef]
34. Radecki, T. Level Fuzzy Sets. *J. Cybern.* **1977**, *7*, 189–198. [CrossRef]
35. Mandelbrot, B.B.; Mandelbrot, B.B. *The Fractal Geometry of Nature*; WH Freeman: New York, NY, USA, 1982; Volume 1.
36. Osborne, A.R.; Kirwan, A.D.; Provenzale, A.; Bergamasco, L. Fractal drifter trajectories in the Kuroshio extension. *Tellus A* **1989**, *41A*, 416–435. [CrossRef]
37. Niazi, A.U.K.; Iqbal, N.; Shah, R.; Wannalookkhee, F.; Nonlaopon, K. Controllability for fuzzy fractional evolution equations in credibility space. *Fractal Fract.* **2021**, *5*, 112. [CrossRef]
38. Al-Sawalha, M.M.; Amir, N.; Shah, R.; Yar, M. Novel Analysis of Fuzzy Fractional Emden-Fowler Equations within New Iterative Transform Method. *J. Funct. Spaces* **2022**, *2022*, 7731135. [CrossRef]
39. Naeem, M.; Rezazadeh, H.; Khammash, A.A.; Shah, R.; Zaland, S. Analysis of the Fuzzy Fractional-Order Solitary Wave Solutions for the KdV Equation in the Sense of Caputo-Fabrizio Derivative. *J. Math.* **2022**, *2022*, 3688916. [CrossRef]
40. Thomson, R.E.; Emery, W.J. *Data Analysis Methods in Physical Oceanography*; Elsevier: Amsterdam, The Netherlands, 2014.
41. Daniel, P.; Jan, G.; Cabioch, F.; Landau, Y.; Loiseau, E. Drift Modeling of Cargo Containers. *Spill Sci. Technol. Bull.* **2002**, *7*, 279–288. [CrossRef]
42. Khan, U.T.; Valeo, C. Dissolved oxygen prediction using a possibility theory based fuzzy neural network. *Hydrol. Earth Syst. Sci.* **2016**, *20*, 2267–2293. [CrossRef]
43. Buckley, J.J. Fuzzy complex numbers. *Fuzzy Sets Syst.* **1989**, *33*, 333–345. [CrossRef]
44. Mandelbrot, B. How Long Is the Coast of Britain? Statistical Self-Similarity and Fractional Dimension. *Science* **1967**, *156*, 636–638. [CrossRef]
45. Blanken, H.; Hannah, C.; Klymak, J.M.; Juhász, T. Surface Drift and Dispersion in a Multiply Connected Fjord System. *J. Geophys. Res. Ocean.* **2020**, *125*, e2019JC015425. [CrossRef]